

✓

**NASA TECHNICAL
REPORT**



NASA TR R-240

C.1

NASA TR R-240

LOAN COPY: RETURN
AFWL (WLIL-2)
KIRTLAND AFB, NM

0068489



TECH LIBRARY KAFB, NM

**BORON CROSS SECTIONS AS
A SOURCE OF DISCREPANCY
FOR CAPTURE CROSS SECTIONS
IN THE KEV REGION**

by Donald Bogart

Lewis Research Center

Cleveland, Ohio

TECH LIBRARY KAFB, NM



0068489

NASA TR R-240

**BORON CROSS SECTIONS AS A SOURCE OF DISCREPANCY FOR
CAPTURE CROSS SECTIONS IN THE KEV REGION**

By Donald Bogart

**Lewis Research Center
Cleveland, Ohio**

NATIONAL AERONAUTICS AND SPACE ADMINISTRATION

For sale by the Clearinghouse for Federal Scientific and Technical Information
Springfield, Virginia 22151 - Price \$1.00

BORON CROSS SECTIONS AS A SOURCE OF DISCREPANCY FOR CAPTURE CROSS SECTIONS IN THE KEV REGION*

by Donald Bogart
Lewis Research Center

SUMMARY

Discrepancies in capture cross sections for gold from 80 to 200 keV are explained by changes in boron ($n\alpha$) cross sections used to monitor neutron fluxes. These changes in boron cross sections are shown to improve agreement in capture data for iodine, indium, silver, antimony, and tantalum. Reexamination of the boron cross section measurements discloses that a modified long counter with considerable loss in efficiency below 200 keV had been used, but its response had been taken to be flat. Boron cross sections, corrected for long counter efficiency, depart significantly from an inverse neutron velocity variation ($1/v$) above ~ 80 keV.

INTRODUCTION

A well-known and frequently discussed dilemma has been the apparent disagreement in the various measurements of neutron radiative capture cross sections in the keV region (refs. 1 to 3). Summarizing a recent symposium, Batchelor (ref. 4) has called attention to the particularly large discrepancies in the capture cross sections for gold and recommended objective studies of these data. Discrepancies for gold are larger than observed for other elements and are more obvious because of the greater overlap in energy region explored by various methods that have used the Bichsel and Bonner (ref. 5) cross section values for boron to monitor neutron flux. For example, the large fund of capture cross sections obtained by Gibbons et al. (ref. 6) with the liquid scintillator tank were measured by using the $B^{10}(n\alpha)Li^{7*}$ cross section values below ~ 160 keV to monitor flux and similarly, the activation data obtained by Cox (ref. 7) have used the $B^{10}(n\alpha)Li^7$, Li^{7*} cross sections below 200 keV to monitor flux.

Other methods independent of boron have been used (refs. 8 and 9) which provide gold cross sections that for the same energies lie in between the two sets based on boron.

*Presented at Conference on Neutron Cross Section Technology, Washington, D. C., March 22-24, 1966.

Inasmuch as all of the experimental procedures have been studied and the discrepancies cannot be ascribed to experimental inadequacies, physical significance must be attributed to these deviations. The question asked here is whether there exists physically plausible corrections to the boron cross sections such that the differences in the gold capture data from 20 to 200 keV are reconciled.

Capture cross sections for gold are presented, and boron cross sections are inferred such that the discrepancies for gold are removed. The resulting energy variation of the boron cross section is used to adjust the scintillator capture tank data (ref. 6) for iodine, indium, silver, antimony, and tantalum. The consistent improvement in agreement of capture data for these isotopes is presented. A probable source of the capture data discrepancies is traced to the boron cross section measurements of reference 5 where a modified long counter had been used whose response function had been taken to be flat but which is believed to have an efficiency that decreases considerably for energies below 200 keV.

CAPTURE CROSS SECTIONS FOR GOLD

The manifold capture cross-section data for gold have been illustrated and discussed by Gibbons (ref. 3). Inasmuch as what is being sought is evidence for systematic inconsistencies in the capture cross sections for gold and other isotopes that may be caused by methods of measurement employing boron as neutron flux monitor, no attempt is made at an evaluation of data. Much of the available data for gold are shown in figure 1. The solid curve represents what is tentatively taken to be the "true" capture cross section.

The activation data of Johnsrud, et al. (ref. 10) above 150 keV, the scintillator tank data of Diven, et al. (ref. 11) above 175 keV, and the activation data of Cox (ref. 7) above 200 keV have used the U^{235} fission cross sections as evaluated by Allen and Henkel (ref. 12) to monitor fast neutron fluxes. Relative cross sections were placed on an absolute basis by Diven by using the known capture plus fission cross section of U^{235} as a reference. Cox employed absolute γ -counting and used the U^{235} fission cross section above 200 keV as an absolute reference; for measurements below 200 keV, Cox employed the $B^{10}(n\alpha)Li^7$, Li^7 cross sections (ref. 5) to monitor neutron flux and the relative cross sections from 30 to 200 keV were normalized to absolute values at 200 keV. Johnsrud avoided the necessity for absolute determination of neutron flux and γ -ray counting efficiencies by comparing fast and thermal neutron induced activities in the same sample. The fast and thermal neutron fluxes were compared with a U^{235} fission counter.

The principal sources of capture data below 200 keV are the scintillator tank data of Gibbons, et al. (ref. 6) for which neutron fluxes were monitored relative to the $B^{10}(n\alpha)Li^7$ cross sections below ~ 160 keV. These capture data were placed on an ab-

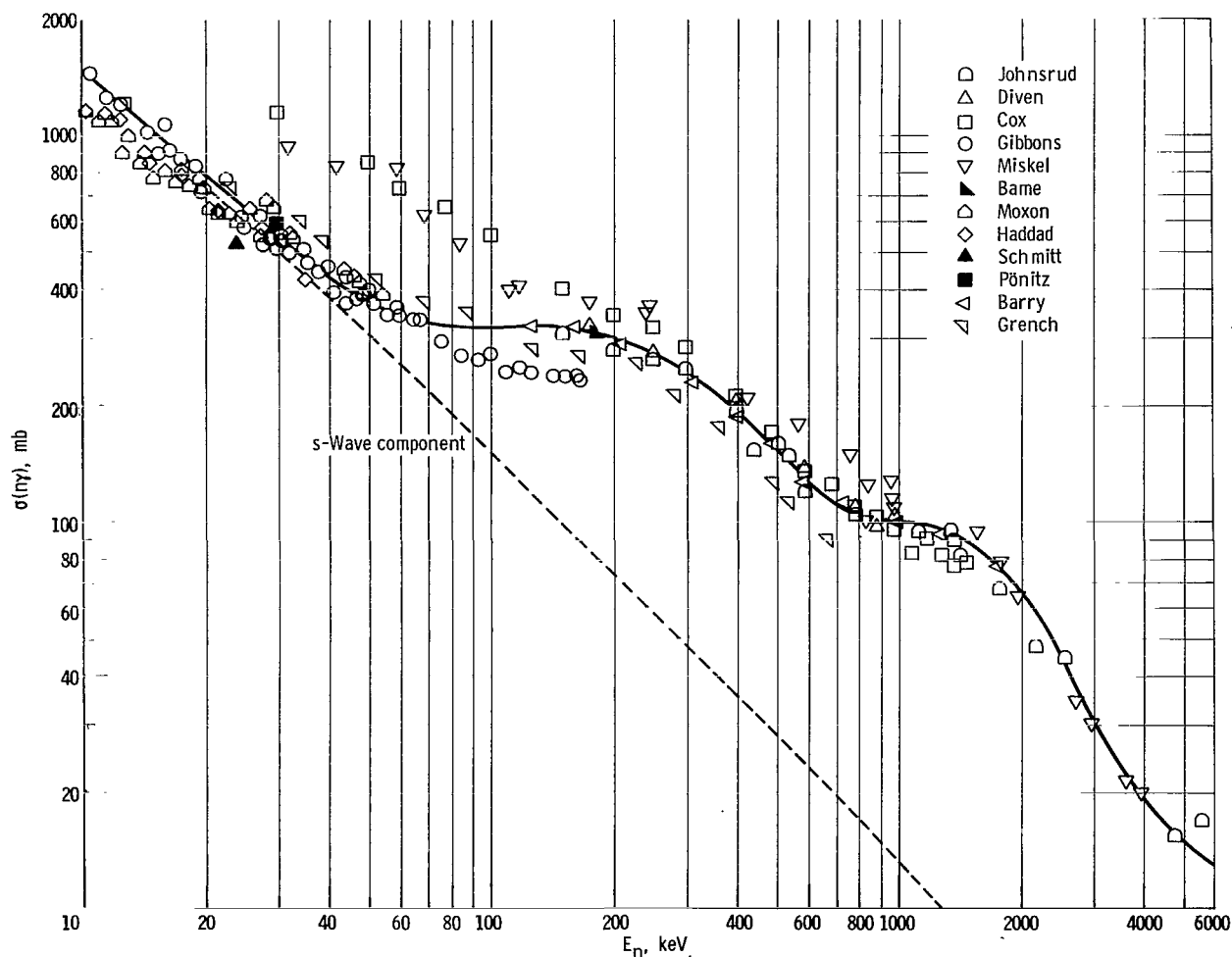


Figure 1. - Capture and activation cross sections for gold-197. s-Wave component calculated using radiation width Γ_γ (0.170 eV), average level spacing \bar{D} (17 eV), s-wave strength function S_0 (1.5×10^{-4}), and potential scattering cross section σ_{pot} (9 b).

solute basis by normalizing to the cross sections at 24 keV as measured by Schmitt and Cook (ref. 13), who used the spherical shell transmission technique; a group normalization was employed that yielded a best fit to the sphere data for gold, iodine, indium, silver, and antimony.

Sphere transmission data are interpreted by a multiple scattering analysis that is strongly dependent on the precision of the average total cross section as well as on the precision of self-shielding corrections for the unresolved resonances that are present. Updated cross sections were reported by Schmitt (ref. 14) for gold. The new value for the capture cross section was given as 532 ± 60 mb at 24 keV based on a total cross section of 13.67 ± 0.28 b. The largest part of the quoted uncertainty in this capture cross section stems from the self-shielding corrections. A direct interpretation of these sphere transmission experiments for gold by a Monte Carlo analysis (ref. 15) provides

a value of 700 ± 50 mb for the capture cross section. In this Monte Carlo analysis, the average s-wave contribution is calculated by using the statistical results from slow neutron resonance spectroscopy as input data. The average p-wave contribution at 24 keV is superimposed as an energy independent capture cross section of such magnitude that the experimental sphere transmission is satisfied. The Monte Carlo study (ref. 15) indicates that difficulties exist with the method of interpretation of sphere transmission measurements at 24 keV.

A measurement by Pönitz (ref. 16) at 30 keV by an activation method provided a value of 598 ± 60 mb for the capture cross section. In this experiment the $\text{Li}(pn)\text{Be}^7$ reaction near threshold was employed as neutron source. The neutron flux was found by absolute determination of the activity of the Be^7 produced in the target.

Two methods that are independent of boron have been employed recently. These methods provide gold cross sections that lie in between those of Cox and of Gibbons in the region below 200 keV. An activation method by Grench, et al. (ref. 8) employed the $\text{V}^{51}(pn)\text{Cr}^{51}$ reaction as a neutron source. The neutron flux was determined by the Cr^{51} activity induced in the V^{51} target. The gold capture rate was determined by absolute γ -counting of the gold samples. Gold cross sections also were measured by Barry (ref. 9) by using an activation method that employed absolute γ -counting of gold discs. The neutron fluxes were measured by U^{235} fission counters that were accurately calibrated relative to the shape and magnitude of the well-known (n-p) scattering cross sections.

Two additional methods, one by Haddad, et al. (ref. 17) using a large liquid scintillator and the other by Moxon and Rae (ref. 18) using a compact scintillation gamma ray detector, have been used with pulsed beam time-of-flight techniques up to ~ 50 keV to measure reaction rates. For these methods, absolute cross sections are dependent on the precision of the determination of the detector efficiency and the absolute neutron flux at the 4.91 electron volts (eV) resonance of gold. Relative neutron fluxes to ~ 50 keV were determined by assuming the $\text{B}^{10}(n\alpha_1)\text{Li}^{7*}$ to vary inversely as neutron velocity ($1/v$).

Finally, some capture cross sections that were measured by activation relative to the U^{235} fission cross sections extend to the energy region below 200 keV. The data of Bame and Cubitt (ref. 19) and of Miskel, et al. (ref. 20) are shown in figure 1 and are considerably higher below 200 keV because they were based on fission cross sections (ref. 12) for both flux monitoring and absolute reference. These fission cross sections are subject to large uncertainties below 200 keV, and the values used are considerably higher than presently preferred values for energies below 200 keV (ref. 21). Consequently, the older data are consistently high for gold and other elements below 200 keV.

Because of the general agreement in gold cross sections above 300 keV and the precision of the Barry (ref. 9) results, the curve representing the "true" gold cross section has been drawn through the Barry data down to 120 keV. This solid curve is extended smoothly into the region below 120 keV passing near the reanalyzed sphere trans-

mission value of 700 mb at 24 keV. The curve is in good agreement with data of Gibbons, et al. (ref. 6), Moxon and Rae (ref. 18), and Haddad, et al. (ref. 17) below 70 keV.

The dashed line in figure 1 indicates the magnitude of the s-wave component obtained from a Monte Carlo calculation (ref. 15) using neutron spectroscopic data for which the average parameters are listed. Comparison with the solid curve indicates a minimal p-wave component but the probable presence of significant d- and f-wave components in the capture cross section for gold.

A clearer picture of the pertinent cross sections for gold is shown in figure 2. The data of Cox (ref. 7) below 200 keV have been renormalized to the data of Gibbons (ref. 6) below 100 keV and both sets are seen to gradually depart from the solid "true" cross section curve for $\bar{\sigma}^{Au}$ that has been drawn to join smoothly with the data of Barry (ref. 9). Since both the Cox data and the Gibbons data used the boron capture data of Bichsel and Bonner (ref. 5) to monitor flux, the ratios $\bar{\sigma}^{Au}/\sigma_{Cox}^{Au}$ and $\bar{\sigma}^{Au}/\sigma_{Gibbons}^{Au}$ may be formed from the data of figure 2 which represents the ratio

$$\frac{\bar{\sigma}^{B^{10}(n\alpha)Li^7, Li^{7*}}}{\sigma_{Bichsel}^{B^{10}(n\alpha)Li^7, Li^{7*}}}$$

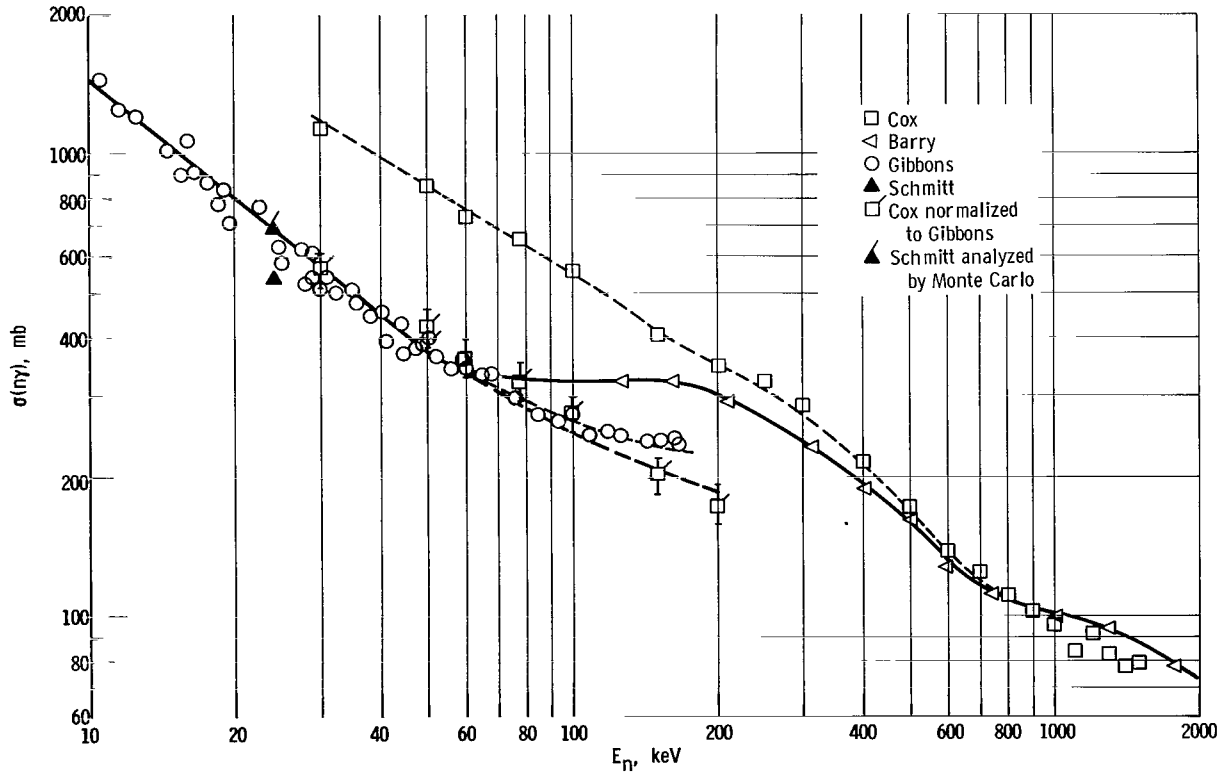


Figure 2. - Capture and activation cross section discrepancies for gold-197.

where the barred values of boron cross sections are the boron cross sections that would make the measured gold capture data agree with the selected "true" values.

The ratios are shown in figure 3 and are seen to increase with energy and to imply significantly increased values of boron cross sections above those used by Cox and Gibbons. Because of the ± 10 percent estimated error in the data on which these ratios are based, it is difficult to ascertain which of the variations shown is more correct, although it seems clear that the boron cross sections can be larger than those reported by Bichsel and Bonner. Boron cross sections are discussed later.

CAPTURE CROSS SECTIONS FOR OTHER ELEMENTS

If the curve in figure 3 representing the cross section ratio $\bar{\sigma}^{\text{Au}}/\sigma_{\text{Gibbons}}^{\text{Au}}$ is correct, it should be universally applicable and should represent the ratio of the "true" capture cross section of any element to the cross section as measured by Gibbons et al. (ref. 6). This ratio has been applied to the capture cross sections for many isotopes and elements and found to improve considerably the agreement of data by the various methods of measurement. The effects on the capture cross sections are discussed for iodine, indium, silver, antimony, and tantalum as examples.

Iodine

Capture cross sections for iodine are shown in figure 4. For the boron based data, no region of overlap exists comparable to gold below 200 keV; however, a discontinuity is apparent in the 100 to 200 keV region. The activation data of Johnsrud, et al. (ref. 10), of Bame and Cubbitt (ref. 19), and of Cox (ref. 22), all of which used the U^{235} fission cross sections to monitor flux, are in reasonable agreement above 200 keV. The data of Bame and Cubbitt (ref. 19) extend down to 20 keV, and while they are in good agreement with other data above 200 keV they are considerably higher below this energy. These data were based on the fission cross sections compiled by Allen and Henkel (ref. 12) that are considerably higher than recently compiled values (ref. 21).

An additional set of data by Gabbard et al (ref. 23) who used a $\text{Li}^6\text{I}(\text{Eu})$ scintillation crystal to measure the integral capture gamma ray rate covers the range from 25 to 500 keV. These cross sections are in very good agreement with the fission based cross sections above 200 keV. In these experiments, the relative neutron flux was monitored by a conventional long counter and placed on an absolute basis by comparison with the flux due to a standard radium-beryllium source.

The principal source of capture data below 200 keV is the scintillator tank data of

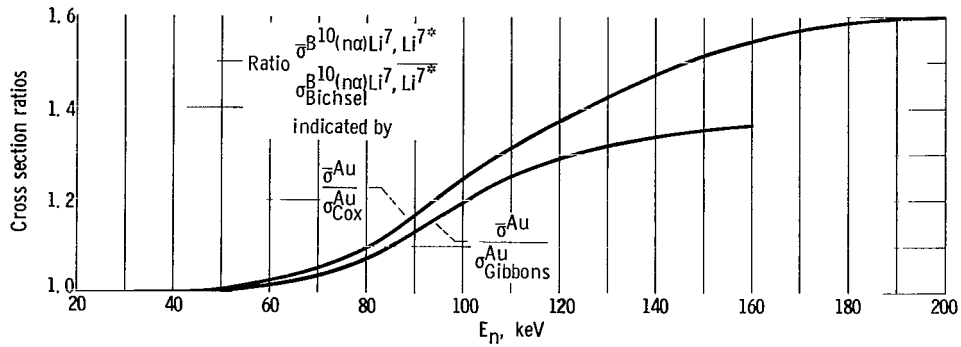


Figure 3. - Boron cross section ratios inferred from gold capture data.

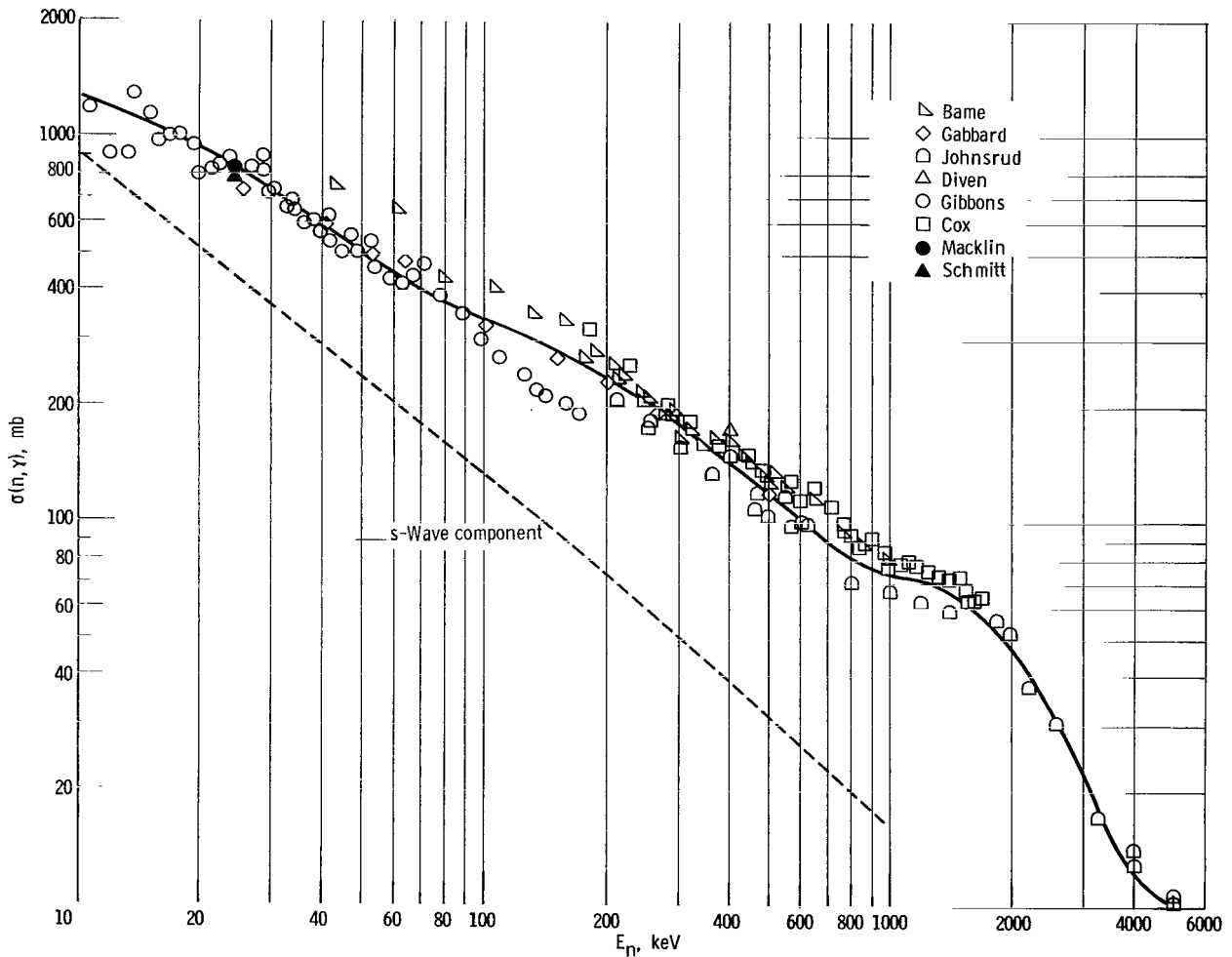


Figure 4. - Capture and activation cross sections for iodine-127. s-Wave component calculated using radiation width Γ_γ (0.107 eV), average level spacing \bar{D} (13 eV), s-wave strength function S_0 (0.69×10^{-4}), and potential scattering cross section σ_{pot} (4 b).

Gibbons et al. (ref. 6). These capture data have been placed on an absolute basis by normalizing to the cross sections at 24 keV as measured by Schmitt and Cook (ref. 13) using the sphere transmission method. An updated capture cross section for iodine was reported by Schmitt (ref. 14) as 768 ± 90 mb at 24 keV based on a total cross section of 6.69 ± 0.36 b. A direct interpretation of the sphere transmission experiment for iodine by a Monte Carlo analysis (ref. 15) indicates a value of 800 ± 80 mb for the capture cross section. These values are in agreement with the value of 820 ± 60 mb obtained by Macklin et al. (ref. 24) by absolute beta-counting a NaI(Tl) crystal in conjunction with a standard antimony-beryllium source to establish neutron flux at the crystal.

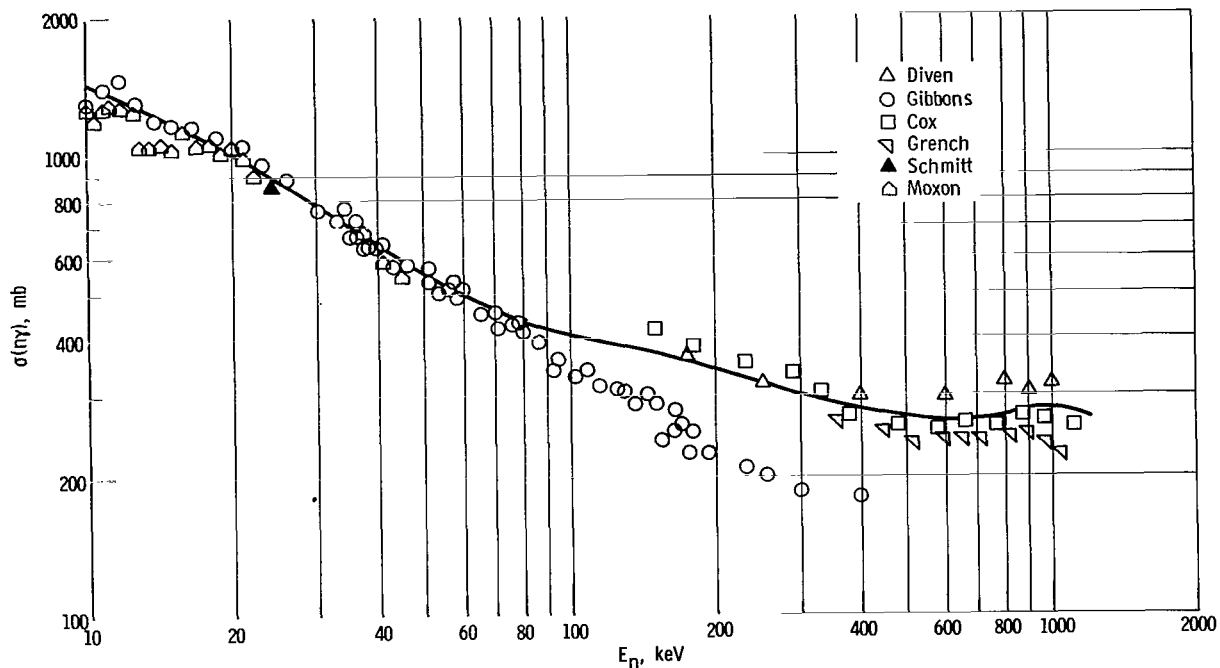
The lower end of the solid curve from 10 to 70 keV follows the scintillator tank data (ref. 6) passing through the value of 820 mb at 24 keV. Between 70 and 160 keV the curve was obtained by multiplying the Gibbons data by the $\bar{\sigma}^{\text{Au}} / \sigma_{\text{Gibbons}}^{\text{Au}}$ cross section ratio curve of figure 3. The resulting curve is seen to join smoothly with the curve that follows an average of the higher energy data. The data of Gabbard et al. (ref. 23) are in remarkably excellent agreement with the solid curve over the entire range of measurement from 25 to 500 keV.

The dashed line on figure 4 indicates the magnitude of the s-wave component obtained from a Monte Carlo calculation (ref. 15) using neutron spectroscopic data for which the average parameters are listed. Comparison with the solid line indicates the probable presence of significant p-, d-, and f-wave components in the capture cross section for iodine.

Indium

Total capture cross sections for indium are shown in figure 5(a). The activation cross sections for formation of the 13-second and 54-minute isomeric activities of In^{115} have been summed and are presented with the scintillator tank total capture data for natural indium. Activation cross sections measured by Grench and Menlove (ref. 25) for the 72-second and 50-day isomeric activities of the 4.3 percent abundant In^{113} indicate the total capture of In^{113} and In^{115} to be approximately equal from 0.4 to 1.0 MeV so that the elemental total capture and isotopic activation data shown in figure 5(b) are directly comparable. Cox (ref. 22) and Grench (ref. 25) observed that the ratio of total-to-54-minute capture cross sections indicated a change in the isomer ratio with energy, increasing from the value of 1.15 (commonly used to normalize 54-minute activity of In^{115} to total capture at low neutron energies) to a value of ~ 1.6 near 200 keV.

A large discrepancy in magnitude is apparent between the scintillator tank data of Gibbons et al. (ref. 6) and the high energy total capture data above 150 keV. The absolute values of indium capture cross section measured in the scintillator tank were nor-



(a) Indium-115. Activation data are sums for 54-minute and 13-second isomers.

Figure 5. - Total capture cross sections.

malized to capture cross sections for monoenergetic neutrons at 30 and 65 keV which, in turn, had been group normalized to the Schmitt and Cook (ref. 13) spherical shell transmission measurements for five elements. The updated capture cross section for indium was reported by Schmitt (ref. 14) as 854 ± 60 mb at 24 keV based on a total cross section of 6.11 ± 0.18 b.

The Moxon and Rae (ref. 18) data are in good agreement with the Gibbons data. The curve that has been drawn passes through the Moxon and Rae data, slightly above the spherical shell transmission value, and follows the Gibbons data to ~ 70 keV. Between 70 and 160 keV, the curve was obtained by multiplying the Gibbons data by the $\frac{\sigma_{\text{Au}}}{\sigma_{\text{Gibbons}}}$ cross section ratio curve of figure 3 (p. 7). The resulting curve is seen to join smoothly with the higher energy data eliminating the discontinuity above 150 keV.

Silver

Capture cross sections for natural silver are shown in figure 5(b). In the energy region below 25 keV are shown the data of Haddad et al (ref. 17) and of Moxon and Rae (ref. 18). Also presented is the updated sphere transmission value at 24 keV reported by Schmitt (ref. 14) of 1127 ± 80 mb that is based on a total cross section of 7.85 ± 0.23 b. The curve that has been drawn follows these data and the scintillator tank data of Gibbons

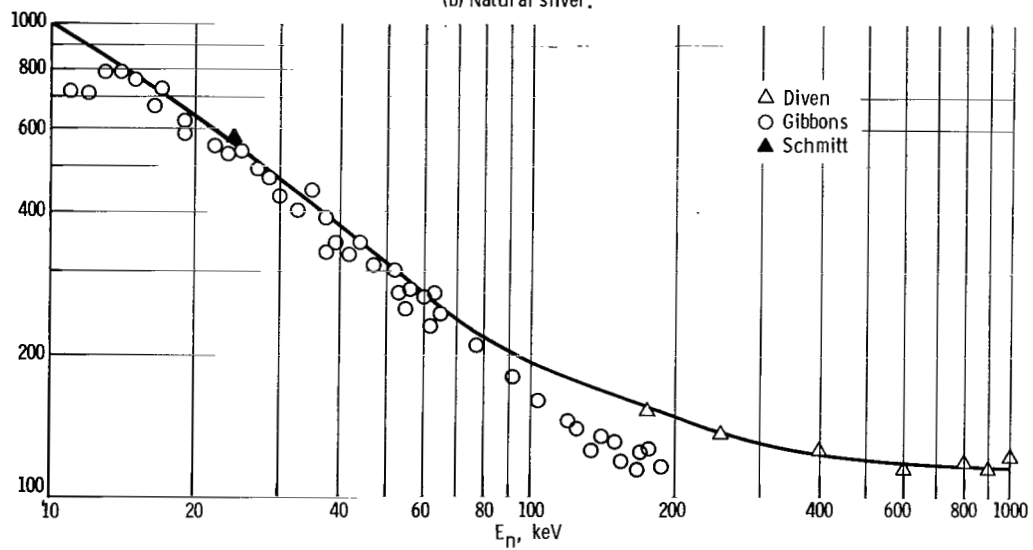
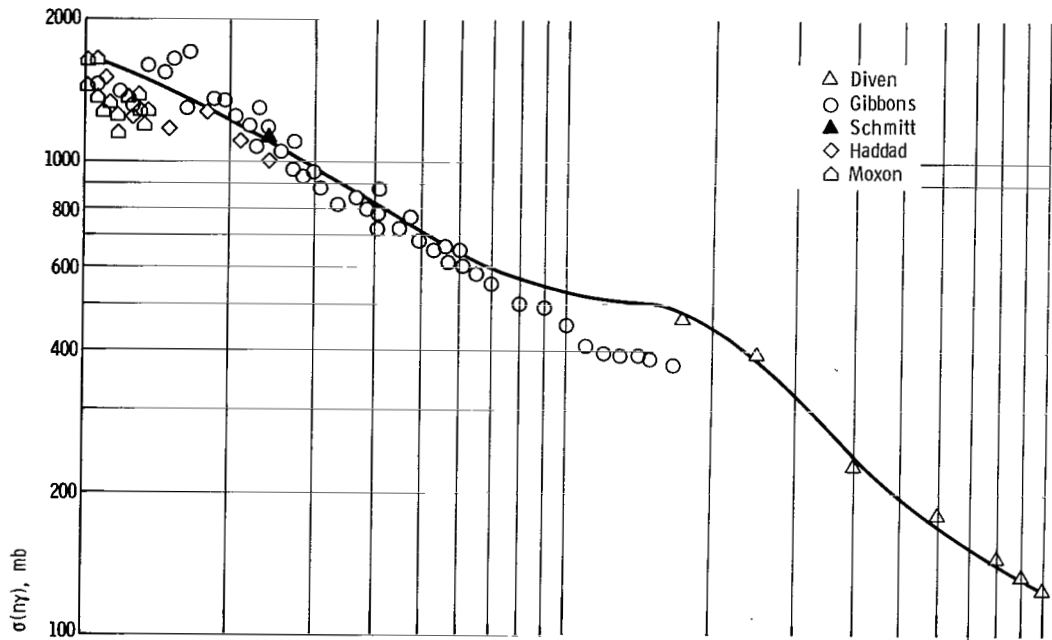


Figure 5. - Concluded.

et al. (ref. 6) up to 70 keV. Between 70 and 160 keV, the curve was obtained by multiplying the Gibbons data by the $\bar{\sigma}^{\text{Au}}/\sigma_{\text{Gibbons}}^{\text{Au}}$ cross section ratio curve of figure 3 (p. 7). The resulting curve is seen to join smoothly with the higher energy data of Diven et al. (ref. 11).

Antimony

Capture cross sections for natural antimony are shown in figure 5(c). The curve that has been drawn passes through the updated sphere transmission value at 24 keV reported by Schmitt (ref. 14) of 578 ± 45 mb that is based on a total cross section of 5.99 ± 0.14 b and follows the scintillator tank data of Gibbons et al. (ref. 6) up to 70 keV. Between 70 and 160 keV, the curve was obtained by multiplying the Gibbons data by the $\bar{\sigma}^{\text{Au}}/\sigma_{\text{Gibbons}}^{\text{Au}}$ cross section ratio curve of figure 3. The resulting curve is seen to join smoothly with the higher energy data of Diven et al. (ref. 11).

Tantalum

Capture and activation cross sections for tantalum are shown in figure 6. The curve that has been drawn follows the data of Moxon and Rae (ref. 18) and that of Gibbons et al. (ref. 6) up to 70 keV. Between 70 and 160 keV, the curve was obtained by multiplying the Gibbons data by the $\bar{\sigma}^{\text{Au}}/\sigma_{\text{Gibbons}}^{\text{Au}}$ cross section ratio curve of figure 3. The resulting curve is seen to join reasonably well with higher energy data of Diven et al. (ref. 11) and of Cox (ref. 22). The fission based data of Miskel (ref. 20) have a large scatter and, as described before, lie generally above the other data in the region from 30 to 150 keV.

PROBABLE SOURCE OF A BORON DISCREPANCY

The reactions studied by Bichsel and Bonner (ref. 5) involving the B^{11} compound nucleus were $\text{Li}^7(\alpha n)\text{B}^{10}$, $\text{Li}^7(\alpha \alpha')\text{Li}^{7*}$, and $\text{B}^{10}(n\alpha)\text{Li}^7, \text{Li}^{7*}$. For detection of the $\text{B}^{10}(n\alpha)\text{Li}^7, \text{Li}^{7*}$ reaction, a BF_3 counter was located 3 centimeters from Li^7 or H^3 targets that served as (pn) neutron sources. The means by which the relative neutron fluxes were monitored for the $\text{B}^{10}(n\alpha)\text{Li}^7, \text{Li}^{7*}$ measurements was not stated explicitly. However, the neutrons from the $\text{Li}^7(\alpha n)\text{B}^{10}$ reaction that was studied were detected with a modified long counter. Direct inquiry confirmed that this modified long counter had been used in both the measurement of differential $\text{Li}^7(\alpha n)$ cross sections and for monitoring relative neutron fluxes in the $\text{B}^{10}(n\alpha)\text{Li}^7, \text{Li}^{7*}$ studies. The efficiency of this modi-

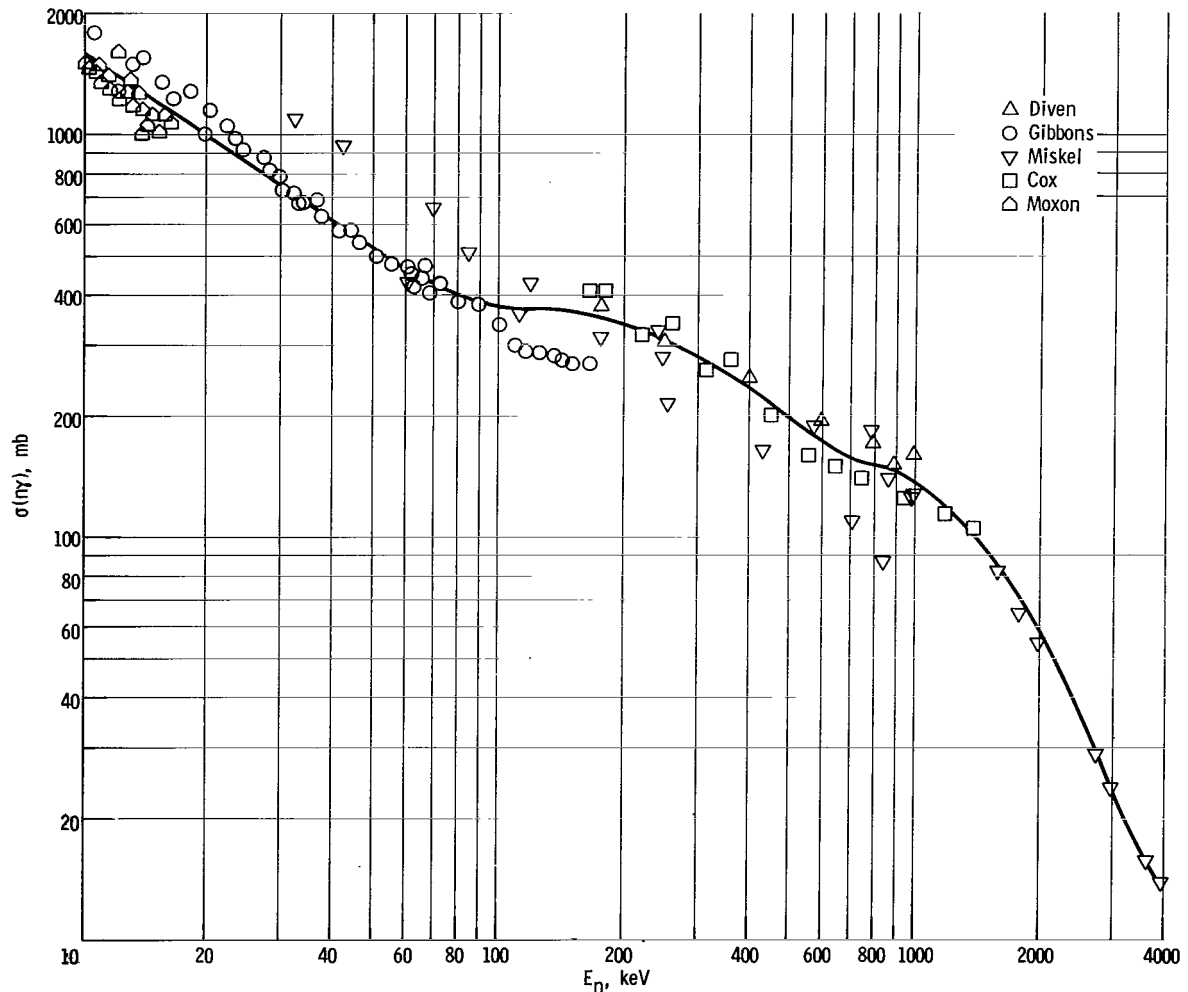


Figure 6. - Capture and activation cross sections for tantalum-181.

fied long counter had been presumed to be flat with energy. Absolute boron cross sections were obtained by normalizing the cross section at 20 keV to a value calculated from the boron cross section at thermal energies and assuming a $1/v$ law to apply.

For a description of the modified long counter used, Bichsel referred to Bonner et al. (ref. 26) from which the following is quoted:

The neutron detector used was a modified long counter with a paraffin moderator 5 inches in diameter and 5 inches long surrounding a BF_3 counter which was 1 inch in diameter and extended to the front surface of the paraffin. This smaller and more compact counter was used in place of a long counter so that considerable angular resolution could be obtained with the counter in a position such that its paraffin face was only 5 inches from the target. Under such geometrical conditions the background counts were small in comparison to the

counts from thin targets of the elements that were investigated. The modified long counter does not have an exactly flat response, independent of neutron energy; its efficiency for counting 4-MeV neutrons is only 60 percent as great as for 1-MeV neutrons.

This modified long counter deviates considerably from a conventional long counter (ref. 27) in both size and response. If the calibration curve for this modified long counter were available, the boron cross sections reported by Bichsel and Bonner could be placed on an absolute basis.

The energy variation of the efficiency of "long counters" is strongly dependent on the amount of paraffin surrounding the BF_3 counter. In fact, a double-walled moderated BF_3 detector was developed for measuring fast neutron dose and flux by DePangher (ref. 28) that exploits the differences in detector sensitivity at various neutron energies. A large loss of efficiency for neutrons below 1 MeV was observed for both of these specially moderated BF_3 detectors.

The modified long counter in question also has been used in a counter-ratio method for the purpose of measuring neutron thresholds as discussed by Marion (ref. 29). This method is also described by Brugger et al (ref. 30) and involves the simultaneous use of two BF_3 counters: one embedded in a paraffin cylinder 5 inches in diameter and 5 inches in length (modified long counter) and the second surrounded by a ring of paraffin 1/2 inch thick and 2 inches in length (slow counter). Both counters are placed at 0° with respect to the direction of the proton beam and subtend approximately the same solid angle at the target. The geometrical arrangement is shown in figure 7.

The efficiency of the two counters was determined simultaneously by observing the counting rate in each of the counters as the energy of the beam of protons striking a LiF target was varied. The results were then compared to the absolute yield into the same cone determined by Taschek and Hemmendinger (ref. 31) in order to find the relative efficiency as a function of neutron energy. The measured efficiency of the modified long

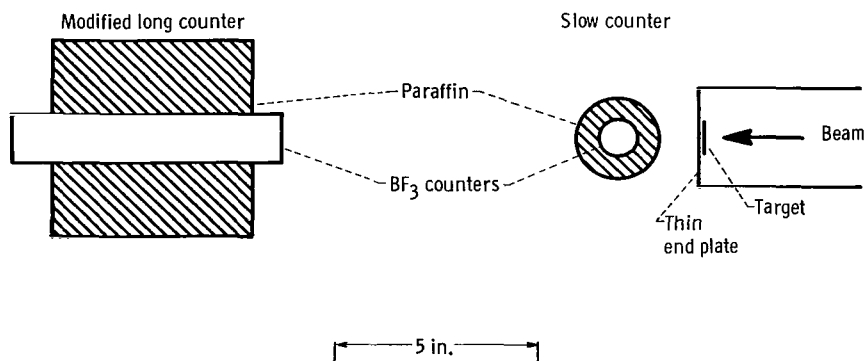


Figure 7. - Detector geometry used at Rice University for counter-ratio threshold measurements (refs. 29 and 30).

counter in its position behind the slow counter is shown by the calibration points in figure 8 and is seen to decrease considerably for neutrons of energy less than 200 keV. Unfortunately, there are no efficiency data at these energies without the slow counter in place. The calibration shown is subject to further uncertainty by virtue of the change in the absolute neutron yields from the $\text{Li}^7(\text{pn})$ reaction in the forward direction that were found to be higher when remeasured by Gabbard et al. (ref. 23); differences in these yields have been discussed by Gibbons and Newson (ref. 32).

The solid and dashed curves in figure 8 from 25 to 200 keV represent the shapes of the efficiency functions required to bring the gold activation cross section data of Cox (ref. 7) and of Gibbons et al. (ref. 6) into agreement with the selected "true" capture cross sections for gold. These curves are seen to lie above the calibration points shown that were obtained by the counter-ratio method but still indicate a considerable loss in efficiency below 200 keV. The efficiency curves merge and are continued to 1 MeV guided by the calibration points and are extended to 4 MeV in accordance with the efficiency value relative to that at 1 MeV cited by Bonner et al. (ref. 26).

CROSS SECTIONS FOR BORON-10

Cross sections for B^{10} above 10 keV are shown in figure 9. The total cross sections are the data of Rohrer (ref. 21) to 80 keV and the data of Bockelman, et al. (ref. 33) who called attention to maxima at 1.8 and 2.8 MeV and to the possibility of a third maxima at 0.2 MeV. Recent total cross sections by Mooring (ref. 34) also indicate a broad maxima near 0.2 MeV.

The $\text{B}^{10}(\text{n}\alpha)\text{Li}^7, \text{Li}^{7*}$ data of Bichsel and Bonner (ref. 5) that are shown are based on the indications of the modified long counter that was presumed to have a flat response. Because of the consistent improvement in the comparison of capture cross sections for many elements, the efficiency curve of figure 8 derived from the shape of the gold data of Gibbons et al. (ref. 6) appears to have validity. The solid curve for the $\text{B}^{10}(\text{n}\alpha)\text{Li}^7, \text{Li}^{7*}$ cross section shown in figure 9 is obtained by correcting the Bichsel and Bonner data by the estimated efficiency curve for the modified long counter as derived from the shape of the gold data of Gibbons et al. The boron cross sections have been normalized to a $1/v$ variation at the lower energies using 3840 b at 0.0253 eV.

By measuring the scattering cross sections and subtracting them from the total cross sections, Mooring (ref. 34) has determined the $\text{B}^{10}(\text{n}\alpha)\text{Li}^7, \text{Li}^{7*}$ cross section. These cross sections are shown in figure 9 and are seen to lie in between the reported and corrected Bichsel and Bonner data. There are suggestions of resonance structure in the data of Mooring near 140 and 220 keV that correspond to the 11.60 and 11.68 MeV levels in B^{11} , respectively.

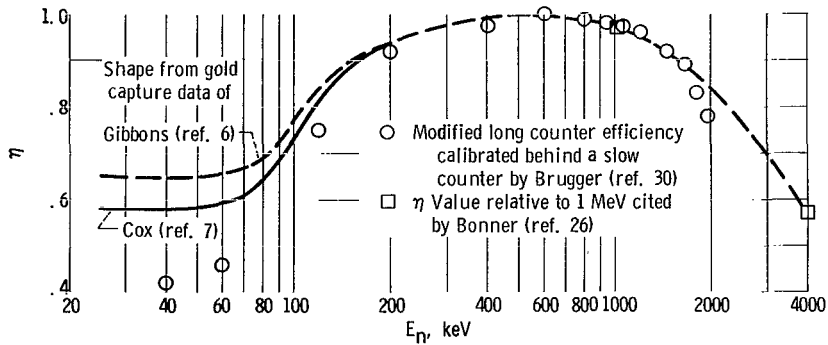


Figure 8. - Estimated efficiency curve for modified long counter.

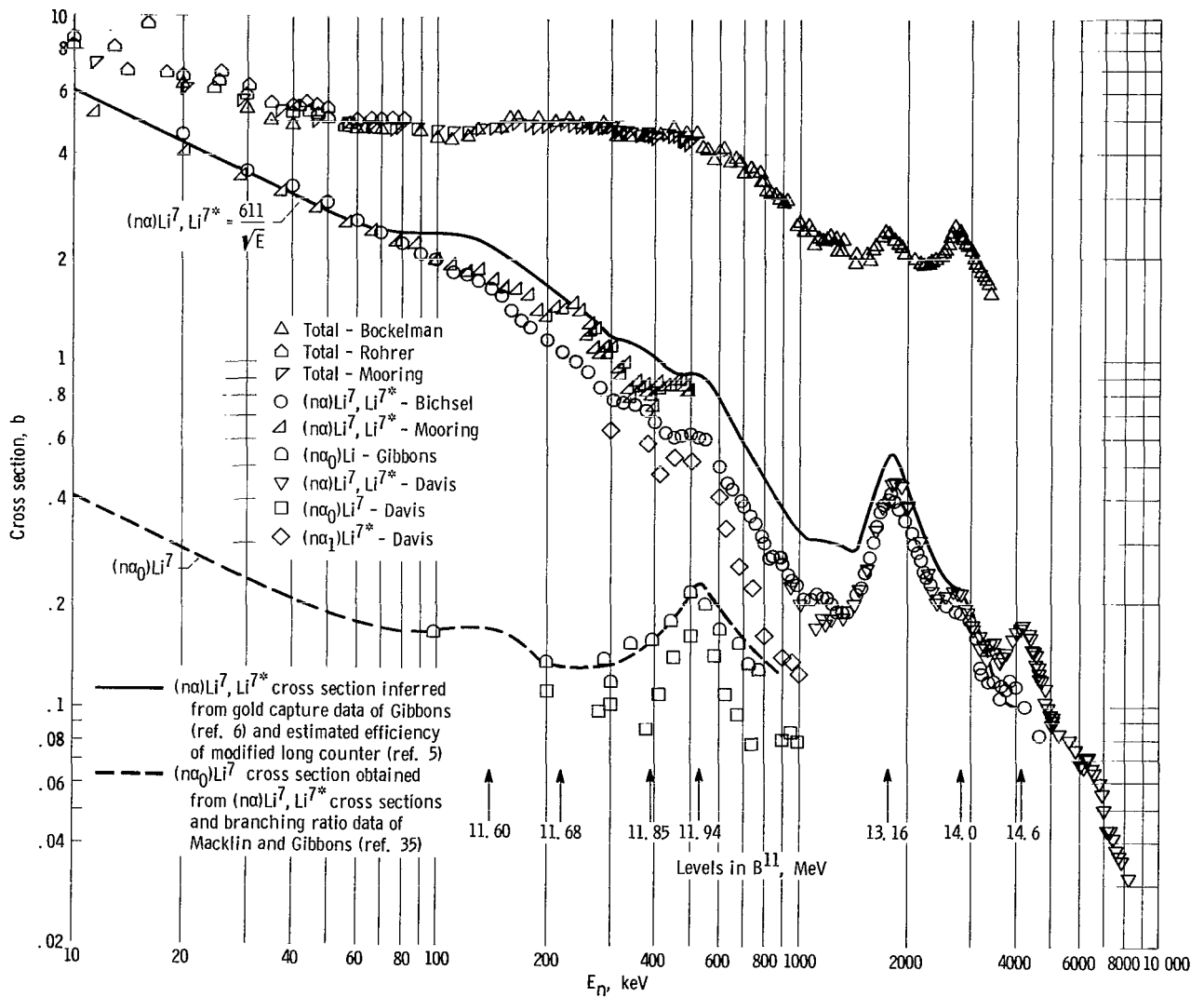


Figure 9. - Cross sections for boron-10.

A separate curve is shown from 10 keV to 1 MeV for the cross section for $B^{10}(n\alpha_0)Li^7$ obtained from the corrected Bichsel and Bonner data by employing the recent branching ratio measurements of Macklin and Gibbons (ref. 35). This curve for $B^{10}(n\alpha_0)Li^7$ clearly shows level structure at 140 and 530 keV and is in remarkably good agreement with the point values of Gibbons and Macklin (ref. 36). These point values of the $B^{10}(n\alpha_0)Li^7$ cross section were calculated by Gibbons and Macklin (ref. 36) from reciprocity using the integral $Li^7(\alpha n)B^{10}$ cross section measurements made with the large 4π graphite spherical detector. These results for $Li^7(\alpha n)B^{10}$ indicated a smoothly increasing cross section from threshold at 4.38 MeV to a peak at 5.15 MeV. However, the differential measurements of $Li^7(\alpha n)B^{10}$ in the forward direction made by Bichsel and Bonner (ref. 5) and repeated recently by Mehta et al. (ref. 37) indicate the cross section to rise from threshold and to exhibit a significant peak in the neighborhood of 4.7 MeV before rising to the peak at 5.15 MeV. Therefore, these differential data suggest resonance structure at alpha particle energies near 4.7 MeV, which corresponds to the level in B^{11} at 11.68 MeV. As Bichsel has suggested, the $B^{10}(n\alpha)Li^7, Li^{7*}$ cross section deviations from the $1/v$ law can be attributed either to a possible level in B^{11} at 11.60 MeV or to the level in B^{11} at 11.68 MeV or both. The 11.60 MeV level was seen

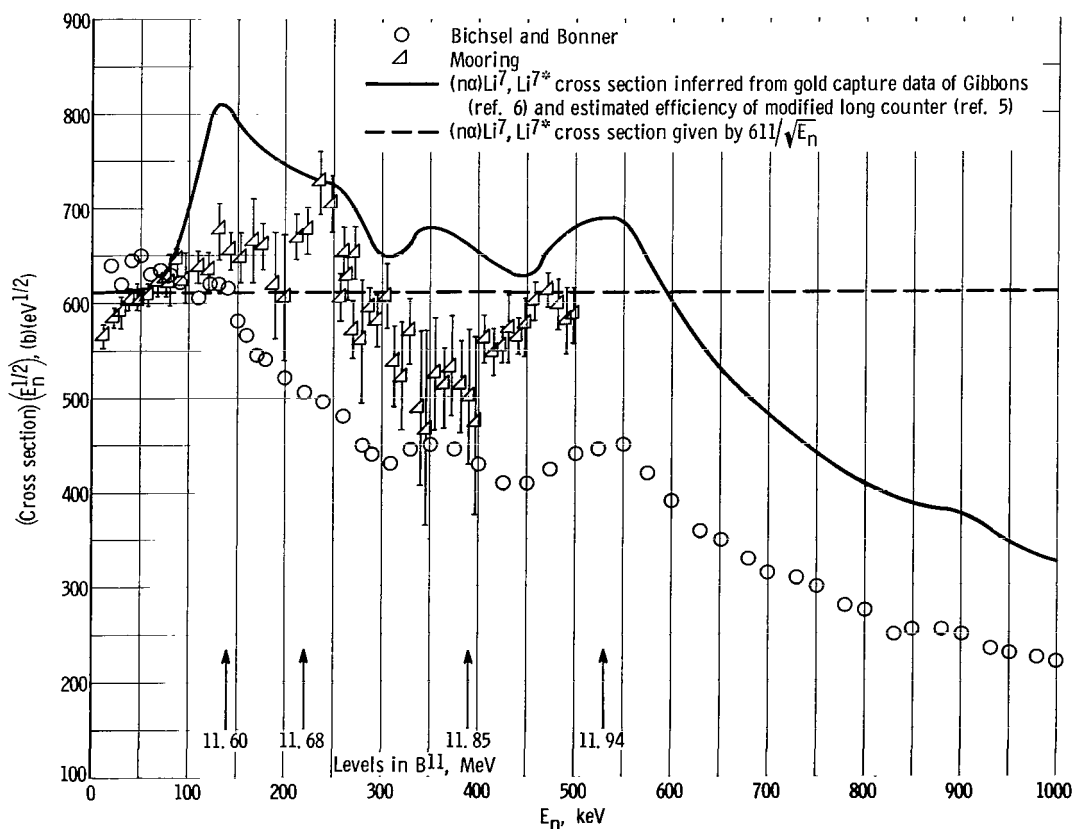


Figure 10. - Comparison of reduced $B^{10}(n\alpha)Li^7, Li^{7*}$ cross sections.

by Bichsel and Bonner in their $\text{Li}^7(\alpha\alpha')\text{Li}^{7*}$ measurements and corresponds to a channel energy of 140 keV in the $\text{B}^{10} + \text{n}$ system. The 11.68 MeV level is seen as the broad resonance at 4.7 MeV in the $\text{Li}^7(\alpha\text{n})\text{B}^{10}$ measurements in the forward direction and corresponds to a channel energy of 220 keV in the $\text{B}^{10} + \text{n}$ system.

Also shown in figure 9 are the cross sections for $\text{B}^{10}(\text{n}\alpha_0)\text{Li}^7$ and $\text{B}^{10}(\text{n}\alpha_1)\text{Li}^{7*}$ as measured by Davis et al (ref. 38) who used a grid-type ionization chamber filled with B^{10}F_3 and argon and performed a pulse-height spectrum analysis. Illustrative spectra presented by Davis for neutron energies at 3.52 and 7.67 MeV show clearly the separation of groups corresponding to $(\text{n}\alpha_0)$ and $(\text{n}\alpha_1)$ for both incident neutrons and for slow epithermal background neutrons. However, as incident neutron energies are reduced to the region below 1 MeV, the separation of the various groups from the background becomes more difficult. The group corresponding to $(\text{n}\alpha_0)$ is least affected by background, but as seen in figure 9, the cross sections fall considerably below the calculated $(\text{n}\alpha_0)$ data of Gibbons and Macklin (ref. 36). This difference is perhaps an indication of background effects at the lower incident neutron energies. These background effects are expected to be even greater for the $(\text{n}\alpha_1)$ group. This is apparent from the summed $(\text{n}\alpha_0 + \text{n}\alpha_1)$ data of Davis which is seen to lie increasingly below the corrected Bichsel and Bonner data for energies below 3 MeV where cross sections are in agreement.

The energy variations in the boron cross sections below 1 MeV are more clearly shown in figure 10 in which the cross sections have been reduced by multiplying by the square root of the neutron energy. The reported data of Bichsel and Bonner (ref. 5) and the values adjusted by the estimated efficiency of the modified long counter that was used are shown. The recent data of Mooring (ref. 34) lie in between the values shown. Resonances corresponding to the 11.60, 11.68, 11.85, and 11.94 MeV levels in B^{11} are apparent. The resonance at a neutron energy of 140 keV is particularly prominent in the corrected cross section curve and introduces a significant departure from a $1/v$ variation above ~ 80 keV.

SUMMARY OF RESULTS

An explanation is offered for disagreements in capture cross sections for gold and other elements in the energy range from 20 to 200 keV. It is shown that the differences for gold capture cross sections that have been measured relative to boron cross sections are reconciled by physically plausible changes in the $\text{B}^{10}(\text{n}\alpha)\text{Li}^7$, Li^{7*} cross sections that are consistent with known resonance structure. The changes in boron cross sections are found to improve considerably the agreement of capture data for many elements; the effects on capture cross sections are illustrated for iodine, indium, silver, antimony, and tantalum. Reexamination of the $\text{B}^{10}(\text{n}\alpha)\text{Li}^7$, Li^{7*} measurements discloses that a modified

long counter with a considerable loss in efficiency below 200 keV had been used, but its response had been taken to be flat. The shape and magnitude changes in the boron cross sections that are required to remove the discrepancies for gold and other elements are found to agree reasonably with changes that result when the approximate efficiency of the modified long counter is considered. The corrected $B^{10}(n\alpha)Li^7, Li^{7*}$ cross sections depart significantly from a $1/v$ variation above ~ 80 keV. The application of recent branching ratio measurements to the corrected data provides values of $B^{10}(n\alpha_0)Li^7$ cross sections in very good agreement with values previously calculated from reciprocity using $Li^7(\alpha n)B^{10}$ data.

Lewis Research Center,
National Aeronautics and Space Administration,
Cleveland, Ohio, March 9, 1966.

REFERENCES

1. Gibbons, J. H.: General Survey on Radiative Capture Measurements by Time-in-Flight. Neutron Time-in-Flight Methods, J. Spaepen, ed., European Atomic Energy Community (Brussels), 1961, pp. 151-166.
2. Cameron, A. G. W.; Lazar, N. H.; and Schmitt, H. W.: Fast Neutron Capture Cross Sections. Fast Neutron Physics, pt. II: Experiments and Theory, J. B. Marion and J. L. Fowler, eds. Vol. IV of Interscience Monographs and Texts in Physics and Astronomy, R. E. Marshak, ser. ed., Interscience Publishers, 1963, pp. 1699-1773.
3. Gibbons, J. H.: Neutron Radiative Capture Reactions. Progress in Fast Neutron Physics, G. C. Phillips, J. B. Marion, and J. R. Risser, eds., University of Chicago Press, 1963, pp. 193-212.
4. Batchelor, R.: Edited Summary of the Symposium. Symposium on the Absolute Determination of Neutron Flux in the Energy Range 1-100 Kev, Sept. 10-13, 1963, held at St. John's College, Oxford, United Kingdom. Rep. No. EANDC-33U, United Kingdom Atomic Energy Authority. Weapons Group. Atomic Weapons Research Establishment, Aldermaston, Berks, England, 1963, pp. 7-13.
5. Bichsel, Hans; and Bonner, T. W.: Reactions $Li^7(\alpha, n)B^{10}$, $Li^7(\alpha, \alpha')Li^{7*}$, and $B^{10}(n, \alpha)Li^7$. Phys. Rev., vol. 108, no. 4, Nov. 15, 1957, pp. 1025-1027.
6. Gibbons, J. H.; Macklin, R. L.; Miller, P. D.; and Neiler, J. H.: Average Radiative Capture Cross Sections for 7- to 170-kev Neutrons. Phys. Rev., vol. 122, no. 1, Apr. 1, 1961, pp. 182-201.

7. Cox, S. A. : Fast Neutron Activation Cross Section of Au¹⁹⁷. Phys. Rev. , vol. 122, no. 4, May 15, 1961, pp. 1280-1282.
8. Grench, H. A. ; Harris, K. K. ; Johnson, R. G. ; and Vaughn, F. J. : The Au¹⁹⁷(n, γ)Au¹⁹⁸ Cross Section. Reports to the AEC Nuclear Cross Sections Advisory Group Meeting Held at National Bureau of Standards, Gaithersburg Laboratory and Atomic Energy Commission Headquarters, Mar. 8-9, 1965, A. B. Smith comp. Rep. No. WASH-1056, Argonne National Lab. , 1965, p. 38.
9. Barry, J. F. : The Radiative Capture Cross Section of ¹⁹⁷Au for Neutrons in the Energy Range 0.12-1.8 MeV. J. Nucl. Energy: Pt. A & B, vol. 18, no. 9, 1964, pp. 491-496.
10. Johnsrud, A. E. ; Silbert, M. G. ; and Barschall, H. H. : Energy Dependence of Fast-Neutron Activation Cross Sections. Phys. Rev. , vol. 116, no. 4, Nov. 15, 1959, pp. 927-936.
11. Diven, B. C. ; Terrell, J. ; and Hemmendinger, A. : Radiative Capture Cross Sections for Fast Neutrons. Phys. Rev. , vol. 120, no. 2, Oct. 15, 1960, pp. 556-569.
12. Allen, W. D. ; and Henkel, R. L. : Fast Neutron Data on the Isotopes of Thorium, Uranium, and Plutonium. Ser. I, Physics and Mathematics, Vol. 2 of Progress in Nuclear Energy, D. J. Hughes, J. E. Sanders, and J. Horewitz, eds. , Pergamon Press, 1958, pp. 1-50.
13. Schmitt, H. W. ; and Cook, C. W. : Absolute Neutron Absorption Cross-Sections for Sb - Be Photoneutrons. Nucl. Phys. , vol. 20, no. 2, Oct. 4, 1960, pp. 202-219.
14. Schmitt, H. W. : Remarks on Absolute Heavy-Element Neutron Capture Cross Sections Determined by the Sphere Transmission Method. Symposium on the Absolute Determination of Neutron Flux in the Energy Range 1-100 Kev, Sept. 10-13, 1963, held at St. John's College, Oxford, United Kingdom. Rep. No. EANDC-33U, United Kingdom Atomic Energy Authority Weapons Group. Atomic Weapons Research Establishment, Aldermaston, Berks, England, 1963, pp. 41-43.
15. Bogart, Donald; and Semler, Thor T. : Monte Carlo Interpretation of Sphere Transmission Experiments for Average Capture Cross Sections at 24 KEV. NASA TR R-239, 1966.
16. Pönitz, W. : The Cross Section of the Reaction Au¹⁹⁷(n, γ)Au¹⁹⁸ for 30 keV Neutrons. Symposium on the Absolute Determination of Neutron Flux in the Energy Range 1-100 Kev, Sept. 10-13, 1963, held at St. John's College, Oxford, United Kingdom. Rep. No. EANDC-33U, United Kingdom Atomic Energy Authority. Weapons Group. Atomic Weapons Research Establishment, Aldermaston, Berks, England, 1963, pp. 164-167.

17. Haddad, E.; Walton, R. B.; Freisenhahn, S. J.; and Lopez, W. M.: Neutron Flux and Capture Measurements Using a Large Liquid Scintillator. Symposium on the Absolute Determination of Neutron Flux in the Energy Range 1-100 Kev, Sept. 10-13, 1963, held at St. John's College, Oxford, United Kingdom. Rep. No. EANDC-33U, United Kingdom Atomic Energy Authority. Weapons Group. Atomic Weapons Research Establishment, Aldermaston, Berks, England, 1963, pp. 114-135.
18. Moxon, M. C.; and Rae, E. R.: A Gamma-Ray Detector for Neutron Capture Cross-Section Measurements. Nucl. Instr. Methods, vol. 24, 1963, pp. 445-455.
19. Bame, S. J., Jr.; and Cubitt, R. L.: (n, γ) Cross Sections of Na^{23} , I^{127} , and Au^{197} . Phys. Rev., vol. 113, no. 1, Jan. 1, 1959, pp. 256-258.
20. Miskel, J. A.; Marsh, K. V.; Lindner, M.; and Nagle, R. J.: Neutron-Activation Cross Sections. Phys. Rev., vol. 128, no. 6, Dec. 15, 1962, pp. 2717-2723.
21. Stehn, John R.; Goldberg, Murrey D.; Wiener-Chasman, Renate; Mughabghab, Said F.; Magurno, Benjamin A.; and May, Victoria M.: Z equals 88 to 98. Vol. No. 3 of Neutron Cross Section. Rep. No. BNL-325 (2nd ed.) (Suppl. 2) (Vol. 3), Brookhaven National Laboratory, Feb. 1965, pp. 92, 235-247.
22. Cox, S. A.: Neutron Activation Cross Sections for Br^{79} , Br^{81} , Rh^{103} , In^{115} , I^{127} , and Ta^{181} . Phys. Rev., vol. 133, no. 2B, Jan. 27, 1964, pp. B378-B383.
23. Gabbard, Fletcher; Davis, Robert H.; and Bonner, T. W.: Study of the Neutron Reactions $\text{Li}^6(n, \alpha)\text{H}^3$, $\text{F}^{19}(n, \gamma)\text{F}^{20}$, and $\text{I}^{127}(n, \gamma)\text{I}^{128}$. Phys. Rev., vol. 114, no. 1, Apr. 1, 1959, pp. 201-208.
24. Macklin, R. L.; Lazar, N. H.; and Lyon, W. S.: Neutron Activation Cross Sections with Sb - Be Neutrons. Phys. Rev., vol. 107, no. 2, July 15, 1957, pp. 504-508.
25. Grench, H. A.; and Menlove, H. O.: $\text{In}^{113}(n, \gamma)\text{In}^{114}(72\text{-sec})$ and $\text{In}^{115}(n, \gamma)\text{In}^{116}(13\text{-sec})$ Fast-Neutron Cross Sections. Bull. Am. Phys. Soc., vol. 9, no. 1, 1964, p. 21.
26. Bonner, T. W.; Kraus, Alfred A., Jr.; Marion, J. B.; and Schiffer, J. P.: Neutrons and Gamma Rays from the Alpha-Particle Bombardment of Be^9 , B^{10} , B^{11} , C^{13} , and O^{18} . Phys. Rev., vol. 102, no. 5, June 1, 1956, pp. 1348-1354.
27. Hanson, A. O.; and McKibben, J. L.: A Neutron Detector Having Uniform Sensitivity from 10 Kev to 3 Mev. Phys. Rev., vol. 72, no. 8, Oct. 15, 1947, pp. 673-677.
28. DePangher, J.: Double Moderator Neutron Dosimeter. Nucl. Instr. Methods, vol. 5, 1959, pp. 61-74.

29. Marion, J. B.: Neutron Threshold Measurements. Progress in Fast Neutron Physics, G. C. Phillips, J. B. Marion, and J. R. Risser, eds., University of Chicago Press, 1963, pp. 23-50.
30. Brugger, R. M.; Bonner, T. W.; and Marion, J. B.: Study of the Nuclear Reactions $\text{Sc}^{45}(\text{p}, \text{n})\text{Ti}^{45}$, $\text{Cu}^{63}(\text{p}, \text{n})\text{Zn}^{63}$, $\text{Cu}^{65}(\text{p}, \text{n})\text{Zn}^{65}$, and $\text{Zn}(\text{p}, \text{n})\text{Ga}$. Phys. Rev., vol. 100, no. 1, Oct. 1, 1955, pp. 84-90.
31. Taschek, Richard; and Hemmendinger, Arthur: Reaction Constants for $\text{Li}^7(\text{p}, \text{n})\text{Be}^7$. Phys. Rev., vol. 74, no. 4, Aug. 15, 1948, pp. 373-385.
32. Gibbons, J. H.; and Newson, Henry W.: The $\text{Li}^7(\text{p}, \text{n})\text{Be}^7$ Reaction. Fast Neutron Physics, pt. I: Techniques, J. B. Marion and J. L. Fowler, eds. Vol. IV of Interscience Monographs and Texts in Physics and Astronomy, R. E. Marshak, ser. ed., Interscience Publishers, 1960, pp. 133-176.
33. Bockelman, C. K.; Miller, D. W.; Adair, R. K.; and Barschall, H. H.: Total Cross Sections of Light Nuclei for p, T-Neutrons. Phys. Rev., vol. 84, no. 1, Oct. 1, 1951, pp. 69-75.
34. Mooring, F. P.; and Monahan, J. E.: Neutron Cross Sections of the Boron Isotopes. Argonne National Laboratory Physics Division Summary Report. Annual Review, April 1, 1964-March 31, 1965. Rep. ANL-7081, Argonne National Lab., 1965, pp. 27-29.
35. Macklin, R. L.; and Gibbons, J. H.: Energy Dependence of the $^{10}\text{B}(\text{n}, \alpha)/^{10}\text{B}(\text{n}, \alpha, \gamma)$ Cross-Section Ratio. Phys. Rev., vol. 140, no. 2B, Oct. 25, 1965, pp. B324-B325.
36. Gibbons, J. H.; and Macklin, R. L.: Total Neutron Yields from Light Elements under Proton and Alpha Bombardment. Phys. Rev., vol. 114, no. 2, Apr. 15, 1959, 571-580.
37. Mehta, M. K.; Hunt, W. E.; Plendl, H. S.; and Davis, R. H.: A Study of the $\text{Li}^6(\alpha, \text{n})\text{B}^9$ and $\text{Li}^7(\alpha, \text{n})\text{B}^{10}$ Reactions. Nucl. Phys., vol. 48, 1963, pp. 90-96.
38. Davis, E. A.; Gabbard, F.; Bonner, T. W.; and Bass, R.: The Disintegration of B^{10} and F^{19} by Fast Neutrons. Nucl. Phys., vol. 27, 1961, pp. 448-466.

"The aeronautical and space activities of the United States shall be conducted so as to contribute . . . to the expansion of human knowledge of phenomena in the atmosphere and space. The Administration shall provide for the widest practicable and appropriate dissemination of information concerning its activities and the results thereof."

—NATIONAL AERONAUTICS AND SPACE ACT OF 1958

NASA SCIENTIFIC AND TECHNICAL PUBLICATIONS

TECHNICAL REPORTS: Scientific and technical information considered important, complete, and a lasting contribution to existing knowledge.

TECHNICAL NOTES: Information less broad in scope but nevertheless of importance as a contribution to existing knowledge.

TECHNICAL MEMORANDUMS: Information receiving limited distribution because of preliminary data, security classification, or other reasons.

CONTRACTOR REPORTS: Technical information generated in connection with a NASA contract or grant and released under NASA auspices.

TECHNICAL TRANSLATIONS: Information published in a foreign language considered to merit NASA distribution in English.

TECHNICAL REPRINTS: Information derived from NASA activities and initially published in the form of journal articles.

SPECIAL PUBLICATIONS: Information derived from or of value to NASA activities but not necessarily reporting the results of individual NASA-programmed scientific efforts. Publications include conference proceedings, monographs, data compilations, handbooks, sourcebooks, and special bibliographies.

Details on the availability of these publications may be obtained from:

SCIENTIFIC AND TECHNICAL INFORMATION DIVISION
NATIONAL AERONAUTICS AND SPACE ADMINISTRATION
Washington, D.C. 20546